Contrasting vegetation productivity responses in arid and humid zones to recent changes in diurnal temperature range

OPEN ACCESS

ARTICLE

The Innovation Geoscience

Contrasting vegetation productivity responses in arid and humid zones to recent changes in diurnal temperature range

Ziqian Zhong,[1] Hans W. Chen,[1,*] Bin He,[2] and Bo Su[2,3]

*Correspondence: hans.chen@chalmers.se

Received: October 28, 2024; Accepted: July 24, 2025; Published Online: August 4, 2025; https://doi.org/10.59717/j.xinn-geo.2025.100163

GRAPHICAL ABSTRACT

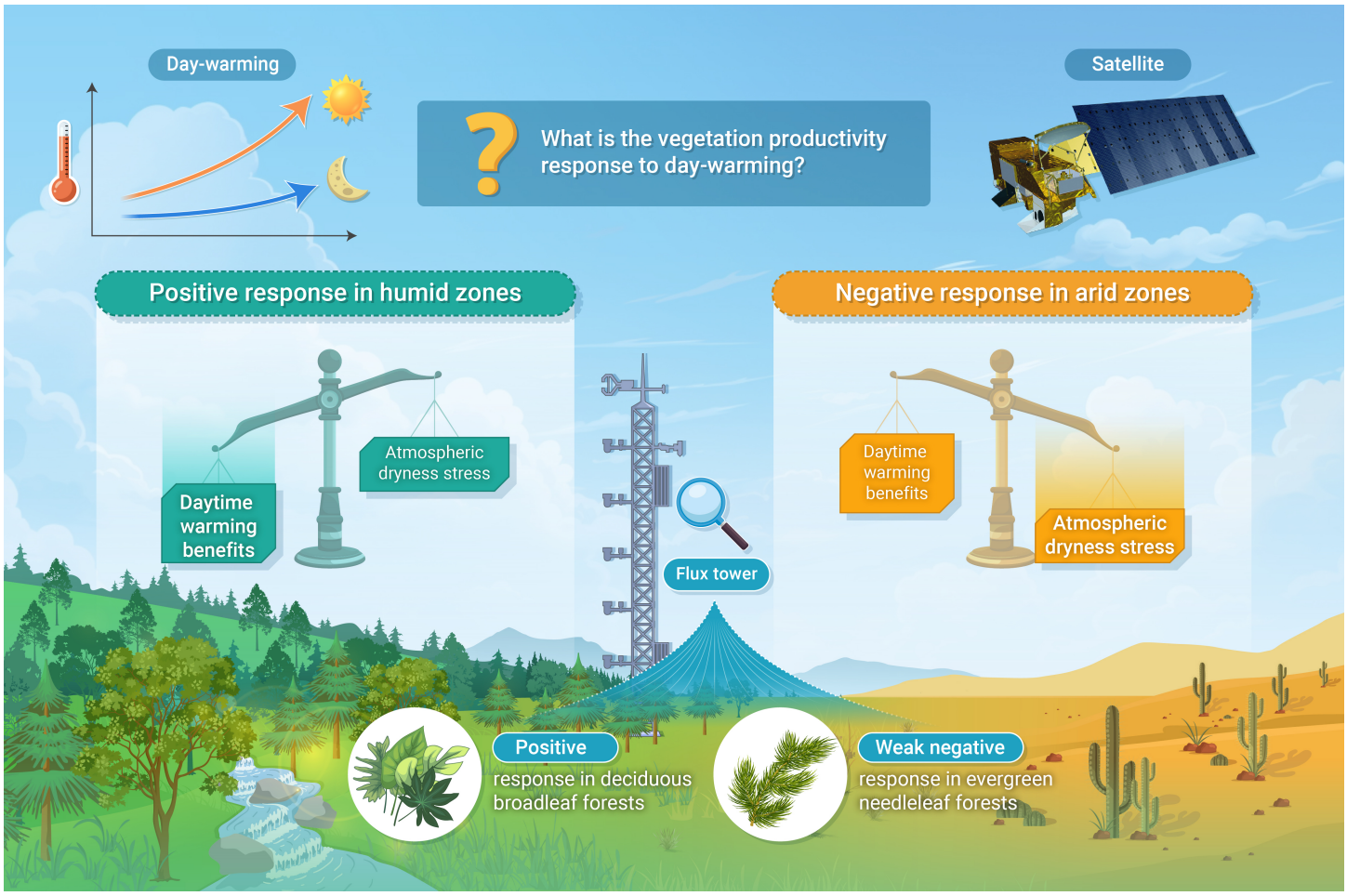

PUBLIC SUMMARY

- Diurnal temperature range (DTR) rose across the extratropical Northern Hemisphere during 2002-2021.
- In humid zones, DTR increases have promoted vegetation productivity.
- Vegetation productivity responds negatively to DTR change in arid zones.
- Broadleaf and needleleaf forest ecosystems show contrasting productivity responses to DTR changes.

ARTICLE

OPEN ACCESS

Contrasting vegetation productivity responses in arid and humid zones to recent changes in diurnal temperature range

Ziqian Zhong,[1] Hans W. Chen,[1,*] Bin He,[2] and Bo Su[2,3]

[1]Department of Space, Earth and Environment, Division of Geoscience and Remote Sensing, Chalmers University of Technology, Gothenburg SE-412 96, Sweden

[2]State Key Laboratory of Earth Surface Processes and Resource Ecology, Faculty of Geographical Science, Beijing Normal University, Beijing 100875, China

[3]Regional Climate Group, Department of Earth Sciences, University of Gothenburg, Gothenburg S-40530, Sweden

*Correspondence: hans.chen@chalmers.se

Received: October 28, 2024; Accepted: July 24, 2025; Published Online: August 4, 2025; https://doi.org/10.59717/j.xinn-geo.2025.100163

Citation: Zhong Z., Chen H. W., He B., et al. (2025). Contrasting vegetation productivity responses in arid and humid zones to recent changes in diurnal temperature range. *The Innovation Geoscience* **3**:100163.

Biological and ecological processes regulating the ecosystem carbon cycle exhibit varying sensitivities to temperature fluctuations during the day and night. Consequently, the diurnal temperature range (DTR)—the difference between daily maximum and minimum temperatures—plays an important role in modulating carbon assimilation and consumption in plants. Over recent decades, daytime warming has outpaced nighttime warming over land, leading to a widening of the DTR, which is expected to impact plant productivity. However, how the recent DTR changes have influenced vegetation productivity across various climate zones remains unclear. Using remote sensing data and flux tower measurements from 2002 to 2021, we found divergent impacts of increased DTR on vegetation productivity in the extratropical Northern Hemisphere. In humid zones, summer DTR increases have promoted net primary production (NPP), while the opposite effect is found in arid zones. This contrast can largely be explained by the larger impact of accelerated daytime warming on increased vapor pressure deficit in arid zones, which consequently inhibits NPP. Our findings underscore the non-negligible impacts of recent DTR changes on vegetation productivity, emphasizing the need to consider sub-diurnal variations in assessments of climate change impacts.

INTRODUCTION

Over the last three decades, global surface temperatures have risen by approximately 0.2°C per decade.[1,2] Nevertheless, the rate of surface warming exhibits variability across different seasons[3,4] and day-night cycles.[5,6] Particularly noteworthy is the asymmetric warming of sub-diurnal temperatures, given its influence on the diurnal temperature range (DTR)—the difference between near-surface daily maximum temperature (T_{max}) and daily minimum temperature (T_{min}). Recent findings indicate that in the past few decades, declining cloud cover and intensified downwelling solar radiation have driven a faster warming rate in T_{max} compared to T_{min} across the Northern Hemisphere (NH) and globally, resulting in increased DTR.[7,8] This signifies the cessation of the "nighttime warming" phenomenon characterized by faster increases in T_{min} than T_{max} during the latter half of the 20th century,[5,9] and the reversal of asymmetric warming over a considerable area of the Earth's land surface. Considering the asymmetric effects of daytime and nighttime warming on vegetation productivity and growth,[10,11] this reversed asymmetric warming has the potential to significantly impact ecosystem carbon absorption and emission processes.

The intricate relationship between T_{max} and T_{min} is crucial for carbon assimilation and consumption in plants. This is because the biological and ecological processes that regulate the ecosystem carbon cycle are influenced by temperature to varying extents during the day and night. Photosynthesis is primarily driven by daytime temperatures, while respiration responds to both daytime and nighttime temperatures.[10,12] The current sub-diurnal asymmetric warming adds complexity to our understanding of how climate warming affects vegetation productivity.[11] On one hand, environmental variables highly correlated with DTR, such as solar radiation and soil moisture (SM),[7,9] also exert influences on vegetation physiological processes, making it difficult to identify the independent effects of DTR on vegetation productivity. On the other hand, the presence of carryover effects between seasons may impede the assessment of how ecosystems productivity has responded to seasonal variations in DTR.[13,14] Consequently, determining the impacts of non-uniform climate warming on terrestrial ecosystems poses a key challenge in carbon cycle research.[11]

The response of terrestrial vegetation productivity to the recent reversal of asymmetric warming of sub-diurnal temperatures remains to be elucidated. In previous scientific inquiries aimed at understanding the effects of asymmetrical warming on vegetation growth or productivity, the conventional methodology often involved separate examinations of the repercussions of T_{max} and T_{min} on vegetation. This analytical framework has advanced our understanding of how variations in T_{max} and T_{min} have influenced vegetation growth.[10–12] However, considering that T_{max} and T_{min} variations encompass a substantial component of the variations in daily mean temperature, this multicollinearity issue could lead to misinterpretations when identifying the impacts of asymmetric warming on vegetation.[15] In contrast, directing attention towards DTR can effectively mitigate this interference and redirect focus towards discerning the effects of differential daytime and nighttime warming rates.

In this study, we investigate how the recent changes in DTR resulting from the reversal of asymmetric warming over the past two decades have impacted the vegetation productivity in the extratropical NH northward of 23.5° N. Seasonal-scale environmental variables, including DTR, will function as independent variables in a regression analysis to assess their impact on annual net primary production (NPP). Acknowledging the role of moisture conditions in determining the impact of DTR changes on vegetation productivity,[16] we conducted separate analyses for dry and wet climate zones (Figure S1A).

MATERIALS AND METHODS

Gridded data

The annual NPP data used in this study were obtained from the Moderate Resolution Imaging Spectroradiometer (MODIS), with a spatial resolution of 500 m, for the period 2002–2021. The MODIS NPP data have undergone rigorous quality control during their generation, including the removal of poor-quality inputs from 8-day Leaf Area Index (LAI) and Fraction of Photosynthetically Active Radiation (FPAR), based on pixel-level Quality Control (QC) flags.[17] To further reduce uncertainty, we calculated the averages of NPP estimated from two datasets, MOD17A3HGF and MYD17A3HGF, based on different satellites. Eight-day solar-induced fluorescence (SIF) data at 0.05° spatial resolution were obtained from the GOSIF product, derived from Orbiting Carbon Observatory-2 (OCO-2) measurements and provided by a previous study.[18] The kNDVI was calculated using NDVI from the MODIS MOD13Q1 dataset following a previous study:[19]

$$\mathrm{kNDVI} = \tanh\left(NDVI^2\right)$$

The FLUXCOM NEE dataset[20] in the RS+METEO setup is a monthly upscaling of carbon fluxes based on machine learning methods driven by eddy covariance, remote sensing, and climate data. In this study, we used the FLUXCOM net ecosystem carbon exchange (NEE, with a negative value indicating net carbon uptake by the land) data based on the fifth generation European Centre for Medium-Range Weather Forecasts climate reanalysis (ERA5) spanning 1980–2018 with a horizontal resolution of 0.5° × 0.5°.

The daily average, minimum, and maximum temperature data were

acquired from the Berkeley Earth Surface Temperatures (BEST) dataset,[21] provided at a spatiotemporal resolution of 1°×1° on a monthly basis spanning from 1850 to the present. This dataset employs sophisticated statistical techniques to quantify and correct measurement biases, ensuring an accurate depiction of global temperature trends. The DTR computed using the BEST dataset demonstrates a robust correlation with the DTR based on the Global Surface Summary of the Day dataset.[7] The monthly incident shortwave radiation (RS) data in all-sky conditions were obtained from the Modern-Era Retrospective analysis for Research and Applications, version 2 (MERRA-2) with a spatial resolution of 0.625° × 0.5° after 1980.[22] The monthly root-zone SM at a spatial resolution of 0.25° was obtained from the Global Land Evaporation Amsterdam Model (GLEAM) version 3.8 dataset.[23]

The aridity index (AI), defined as the ratio of annual precipitation to annual potential evapotranspiration, was used to identify global climate zones. Under this quantitative indicator, the extratropical NH was classified into arid (AI<0.2), semi-arid (0.2≤AI<0.5), semi-humid (0.5≤AI<0.65), and humid (AI≥0.65) zones. The aridity index was obtained from the Global Aridity Index and Potential Evapotranspiration (ET0) Climate Database v3.[24] All gridded datasets were aggregated to a spatial resolution of 0.5° × 0.5°.

Flux tower measurements

The flux tower observations of temperature, shortwave radiation and NEE were obtained from FLUXNET2015[25] and the Integrated Carbon Observation System (ICOS) network.[26] These datasets underwent meticulous quality control, filtering, gap-filling, and partitioning procedures. Only time series encompassing complete observations over at least a two-year period were selected for analysis, and included air temperature, shortwave radiation, atmospheric vapor pressure deficit (VPD) and NEE. The DTR at each flux tower site was determined using half-hourly temperature observations, with the day's DTR being defined as the difference between the daily maximum and minimum temperatures. Monthly values were subsequently computed by averaging the daily values. The variable "NIGHT" was used to delineate daytime and nighttime. Considering the substantial gaps in SM data from measurements around flux towers, we used the GLEAM version 3.8 dataset as an alternative for SM at the tower sites.

The spatial distribution of the flux tower sites in humid zones is sparse, with limited numbers for evergreen broadleaf forest (1 site), open shrub (4 sites), and closed shrub (2 sites). Due to the limited number of flux tower sites in arid zones, with only 3 grassland sites, we extended our study to the entire arid and semi-arid zones, focusing on the grassland vegetation type in these water-limited areas.

HadISD observational data

HadISD[27] is an in-situ sub-daily dataset based on the NOAA ISD dataset.[28] Several quality control procedures have been implemented in the dataset, including checks for duplicates, distribution gaps, and climatological outliers.[27,29] For station selection, we applied strict criteria to temperature and relative humidity data: a day is considered valid if there are at least 5 observations of both temperature and relative humidity, otherwise, it is marked as missing; a month is discarded if there are more than 11 missing days overall or if 5 or more consecutive days are missing;[8] for the period from 2002 to 2021, only stations with no missing months during the summer (June-July-August) were included. After selection, 910 stations in the extratropical NH were retained for analysis.

Seasonal analysis

To analyze DTR variations by season, we used meteorological seasons in the NH: spring (March, April, May), summer (June, July, August), autumn (September, October, November), and winter (December, January, February). Correspondingly, the annual average value of a monthly variable in one year is defined as the average of 12 months from December in the preceding year to November of that year.

Ridge regression and attribution

Ridge regression was crucial in minimizing the impact of high multicollinearity among the independent variables on the regression results, particularly reducing interference from strong correlations between different variables such as DTR, solar radiation, and SM,[7] as well as mitigating the high seasonality-related correlations of the variables. In the ridge regressions, a total of 16 independent variables were considered, including mean temperature, solar radiation, SM, and DTR for each of the four seasons. Prior to performing the ridge regression analysis, all time series were standardized to z-scores by subtracting their climatology means and dividing by their climatological standard deviations from 2002 to 2021.

The ridge regression objective function can be expressed as follows:

$$\beta^{\wedge} = \sum_{i=1}^{n} \left(y_i - \beta_0 - \sum \beta_i x_i\right)^2 + \lambda \sum \beta_i^2$$

where $\beta^{\wedge}$ represents the estimated regression coefficients, y_i is the dependent variable, β_0 is the intercept term, and β_i signifies the regression coefficient for the independent variable x_i. The last term serves as a penalty term added to the least squares objective function during model fitting. It encourages the regression coefficients to shrink towards zero while still preserving their relationship with the predictors. Throughout the regression analysis process, the initial value of λ was set to 0 and incremented by a step size of 0.01. As λ increased, the degree of multi-collinearity decreased. The increment of λ stopped when the Variance Inflation Factor value dropped below 3, with this λ value being determined as the tuning parameter at this grid point.[7]

Based on the ridge regression coefficients, the relative contribution rate η_i of each predictor F_i was estimated as follows:

$$"\eta_i = \frac{|\beta_i|}{\sum_i^n |\beta_i|} \times R^2$$

where R^2 is the R-squared value of the ridge regression model.

Principal components regression

We employed principal components regression analysis to verify the influence of environmental variables on NPP.[30] This method transforms the original dataset into a new set of orthogonal (i.e., uncorrelated) variables, known as principal components (PCs). Following this transformation, a least squares regression was conducted on the reduced set of PCs. Principal components regression effectively mitigates collinearity among climatic variables since the PCs are uncorrelated with one another.[31] PCs that account for low variance in the original predictors indicate potential collinearity and should be excluded from the regression analysis. Specifically, we excluded PCs that explain less than 5% of the total variance in NPP.[31,32] The significance of the principal components regression analysis was evaluated using an F-test with a significance level of 0.05.

Random forest regression

We also employed the random forest algorithm to assess the impact of DTR changes on NPP. The input for the random forest was standardized in a manner consistent with the ridge regression analysis. During the modeling process at individual grid cells, the random forest model was trained using 100 decision trees based on the same data as for the ridge regression analysis. Each decision tree independently predicted annual NPP values based on the given predictor variables. Furthermore, we applied out-of-bag prediction error estimation, an intrinsic capability of the random forest algorithm, and evaluated the importance of the predictors using the out-of-bag predictor importance feature. Similar to the ridge regression coefficients, these feature importances of predictors were subsequently employed to quantify the contributions of seasonal temperature, solar radiation, SM, and DTR to annual NPP.

Structural equation modeling

Structural equation modeling is a multivariate statistical technique used for path analysis, leveraging prior knowledge to establish relationships among variables. The theoretical foundation for the hypothetical relationships in this study is as follows: (1) Solar radiation reaches the Earth's surface, where part of it is absorbed and converted into heat, raising the surface temperature. This heating effect primarily occurs during the day, while its impact on T_{min} mainly results from the lagged effect of daytime warming. As a result, solar radiation has a greater influence on T_{max} than on T_{min}.[33,34] Solar radiation

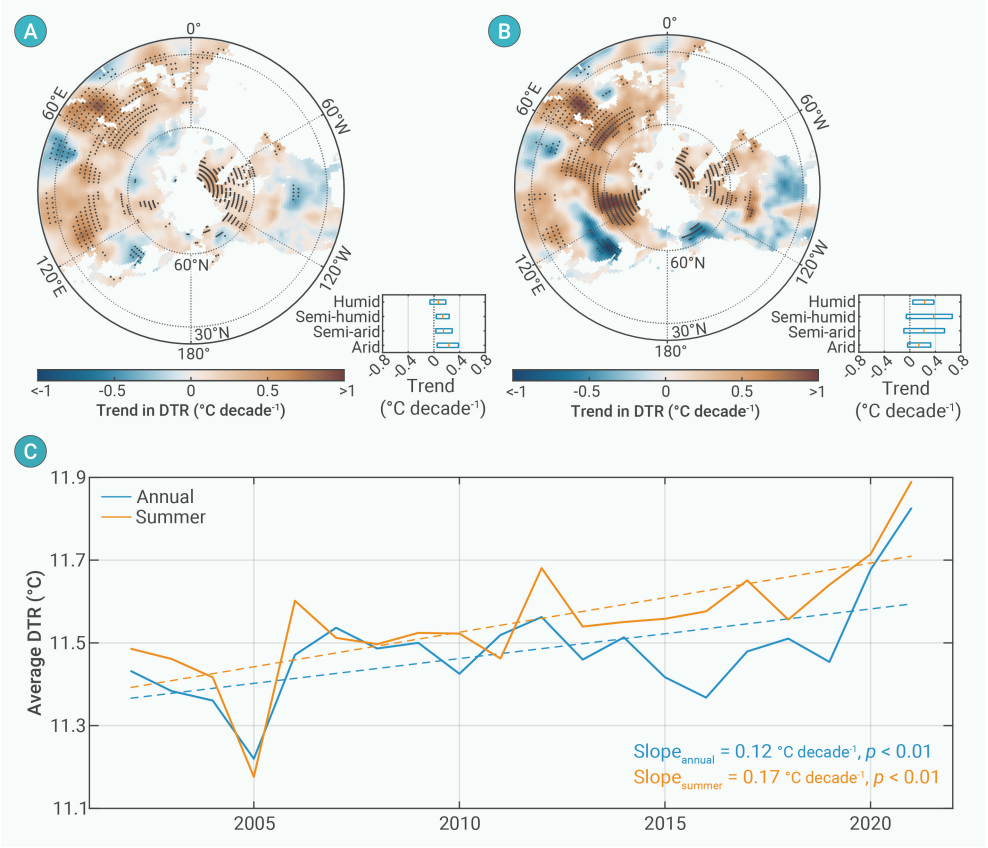

Figure 1. Trend in diurnal temperature range (DTR) in extratropical Northern Hemisphere (A) and (B) Spatial distribution of the trend in annual (A) and summer (B) DTR during 2002–2021. The black dots mark the areas where the trends are significant at the p<0.1 level. The insets show the DTR trends in humid, semi-humid, semi-arid, and arid zones with a boxplot. The width of each box indicates the interquartile range of the trends for all grid points, the red line within each box represents the median, and the left and right edges of the box indicate the first and third quartiles, respectively. The spatial distribution of the four climate zones is illustrated in Figure S1A. (C) Variations and changes in area-averaged annual and summer DTR over land in the extratropical Northern Hemisphere from 2002 to 2021. The dashed lines show the linear trends in DTR obtained from linear regressions.

intensity also influences the rate of photosynthesis, which in turn affects NPP and NEE. (2) SM serves as the primary water source for plants, dictating how much water plant roots can extract.[35] Low SM availability is commonly used to identify drought stress in vegetation, and has been shown to accurately capture the effects of drought on vegetation productivity.[36] (3) Temperature directly affects key physiological processes in plants, including photosynthesis, respiration, transpiration, and cell formation.[37–39] Photosynthesis is mainly influenced by T_{max} as it occurs primarily during daylight hours, whereas respiration occurs continuously, making it sensitive to both T_{max} and T_{min}.[11] (4) Interactions between key environmental variables are also present. For instance, both solar radiation and temperature influence SM through their effects on evapotranspiration.[40] In turn, SM impacts solar radiation by influencing cloud formation,[41] while the evaporative cooling effect of SM can also lower temperature.[42]

All variables were transformed into z-scores prior to conducting the path analysis. We employed maximum likelihood estimation for parameter estimation in the structural equation modeling. Model fit was assessed using multiple criteria, including the comparative fit index (CFI), adjusted goodness of fit index (AGFI), and root mean square error of approximation (RMSEA).

Vapor pressure deficit variation and its relationship with diurnal temperature range

Based on the HadISD observational data, VPD (hPa) was calculated using the following formula:[43]

$$\mathrm{VPD} = e_s \times (1 - RH/100)$$

$$e_s = 6.112 \times f_w \times e^{\frac{17.67T_a}{T_a+243.5}}$$

$$f_w = 1 + 7 \times 10^{-4} + 3.46 \times 10^{-6} P_{mst}$$

$$P_{mst} = P_{msl}\left(\frac{T_a + 273.16}{T_a + 273.16 + 0.0065 \times Z}\right)^{5.625}$$

Here, e_s is the saturation vapor pressure calculated based on the temperature (T_a) in degrees Celsius and the altitude (Z) in meters using the Clausius–Clapeyron relationship. RH is the relative humidity in percent, P_{mst} is the air pressure in hPa, and P_{msl} is the air pressure at mean sea level (1013.25 hPa).

Using daily averaged temperature and relative humidity, we calculated the daily VPD (VPD_{daily}) following the equation above. In contrast, $VPD_{subdaily \to daily}$ was obtained by averaging multiple sub-daily VPD values derived from sub-daily temperature and relative humidity values. The difference between $VPD_{subdaily \to daily}$ and VPD_{daily} is denoted as ΔVPD. The linear response of ΔVPD to DTR ($\Delta VPD/DTR$) was quantified using the following equation:

$$\frac{\Delta VPD}{DTR} = R.c. \times R^2$$

where $R.c.$ is the regression coefficient and R^2 is the R-squared value of the regression model, with DTR (°C) as the independent variable and ΔVPD (hPa) as the dependent variable.

RESULTS

Recent diurnal temperature range change in the extratropical Northern Hemisphere

First, we examined the spatiotemporal trends in DTR changes from 2002 to 2021. Across the extratropical NH, the annual mean DTR over land areas exhibited a significant (p<0.01) increase at a rate of 0.12°C decade^{-1} (Figure 1). When scrutinized seasonally, the most pronounced rise was identified during boreal summer, reaching 0.17°C decade^{-1} (p<0.01), followed by spring (0.14°C decade^{-1}, p<0.05), and winter (0.12°C decade^{-1}, p<0.1), with autumn displaying a non-significant (p>0.1) increasing trend (Figure S2). Regionally, owing to the faster warming rate of T_{max} compared to T_{min} (Figures S1E & I), the increase in summer DTR was particularly conspicuous in semi-humid zones, followed by humid and semi-arid zones. In spring and winter, the strongest increase in DTR occurred in arid and semi-arid zones. Considering that summer represents the peak season for plant photosynthesis in northern ecosystems,[44] the asymmetrical warming phenomenon characterized by a predominant increase in summer DTR over the past two decades is likely to have impacted vegetation productivity in the extratropical NH, especially in temperature-constrained regions such as the humid and semi-humid zones.

The impact of recent diurnal temperature range change on vegetation productivity

To evaluate the influence of DTR changes on NPP, we employed ridge regression using seasonally mean DTR, air temperature, solar radiation, and SM for the four seasons as independent variables, and annual NPP estimates from the Moderate Resolution Imaging Spectroradiometer (MODIS)[45] as the dependent variable (Figure S3). Air temperature, solar radiation, and

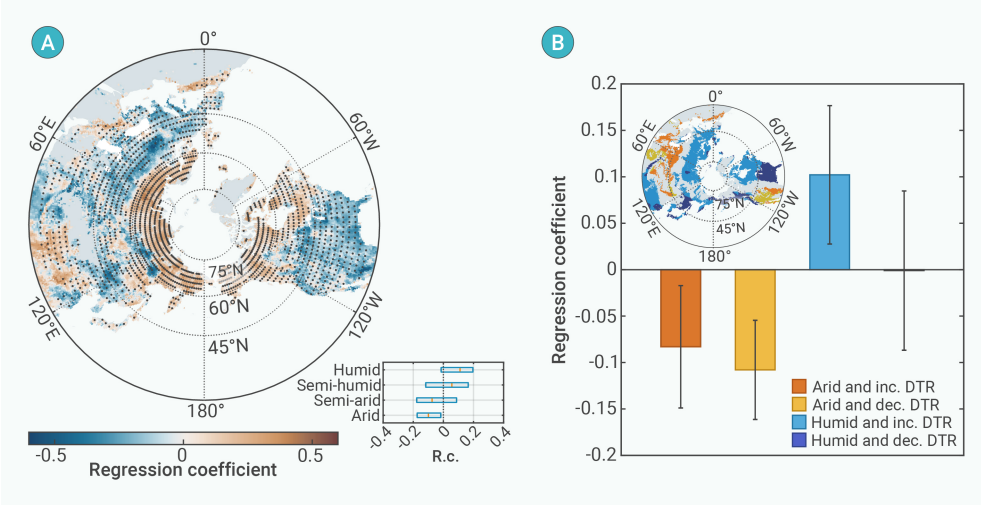

Figure 2. Impact of summer diurnal temperature range (DTR) on vegetation productivity (A) Spatial distribution of ridge regression coefficients of summer DTR to annual net primary production (NPP) from 2002 to 2021. The black dots mark the areas where the regression results are significant at the $p<0.05$ level. The inset shows the regression coefficients (R.c.) across different climate zones with a boxplot. The width of each box indicates the interquartile range of the regression coefficients for all grid points, the red line within each box represents the median, and the left and right edges of the box indicate the first and third quartiles, respectively. (B) Ridge R.c. of NPP with summer DTR in four regions: arid zones with increasing (inc.) DTR, arid zones with decreasing (dec.) DTR, humid zones with inc. DTR, and humid zones with dec. DTR. The inset shows the spatial distribution of these four regions.

SM are key environmental factors that regulate vegetation growth. Using seasonal environmental variables alongside annual NPP enables us to capture carryover effects,[13,14] such as the influence of environmental conditions in one season (e.g., spring) on NPP in subsequent seasons (e.g., summer and autumn). Given the inherent correlations among these seasonal variables, ridge regression was essential to mitigate the effects of multicollinearity among the predictors. The regression results show that in the summer season, which experienced the most pronounced DTR increase, opposite NPP responses to DTR changes occurred in arid and humid zones (Figure 2A). Specifically, there was an overall positive NPP response to DTR increases in humid zones, while the NPP response in arid zones was predominantly negative. We delved further into exploring whether DTR increases or decreases led to differential impacts on NPP (Figure 2B). In arid zones, regardless of whether summer DTR increased or decreased, annual NPP showed a negative response to summer DTR changes. Conversely, in humid zones, encompassing areas with increased summer DTR such as southern China, the high latitudes of the Eurasian continent and North America, a widespread positive impact of summer DTR increases on annual NPP is observed. However, in regions such as the eastern United States where summer DTR has decreased, the influence of summer DTR on annual NPP shows less distinct positive or negative characteristics. Across much of the eastern United States, there is no significant increase in either summer DTR (Figure 1B), T_{max} (Figure S1E), or T_{min} (Figure S1I), indicating a lack of substantial regional warming[46] and sub-diurnal asymmetric warming during the study period. This could limit the influence of mean temperature and DTR changes on vegetation productivity in the eastern United States.

The above findings suggest that in humid zones, the increased DTR has positively influenced vegetation productivity. Daytime warming can enhance plant carbon uptake by aligning the temperature closer to the optimum for photosynthesis. Meanwhile, the relatively slower rate of nighttime warming is conducive to mitigating carbon emissions resulting from respiratory processes.[11] Therefore, an increase in DTR is conducive to carbon absorption in humid zones. In contrast, in arid zones where vegetation faces water limitations, the rise in DTR often coincides with higher daytime temperatures and increased VPD,[31] prompting vegetation to close their stomata, which hinders photosynthesis and carbon uptake.[47-49]

In order to delineate the extent of the impact of summer DTR variations on annual NPP, we quantified the relative contributions of DTR to NPP in both humid and arid zones (Figure 3). Here, the relative contribution was derived using the ridge regression coefficients, normalized by the sum of the absolute values of all coefficients and scaled by the model's R-squared value. The results reveal that in humid zones, the average contribution of summer DTR variations to annual NPP variations was 6.5 ± 4.1%. While this value is lower than the contributions of summer solar radiation (10.1 ± 4.9%) and summer temperature (9.9 ± 6.0%), it is around the contributions of spring temperature (6.4 ± 4.2%) and spring solar radiation (5.2 ± 3.4%) to annual NPP, indicating a non-negligible positive influence of DTR variations on NPP. Conversely, in arid zones, the average contribution of summer DTR variations to annual NPP was 5.2 ± 3.7%, lower than the contribution from summer temperature (6.7 ± 4.8%), but close to that of summer solar radiation (5.4 ± 3.6%).

Responses of different ecosystems to diurnal temperature range change

We employed flux tower measurements to analyze the effect of summer DTR on annual NEE (with a negative value indicating net carbon uptake by the land) in various ecosystems within the different zones of the extratropical NH. First, we focus on the impact of DTR on NEE within the two most common forest ecosystem types in the humid zones of the extratropical NH, namely deciduous broadleaf forests (DBF) and evergreen needleleaf forests (ENF).[50] A significant negative linear correlation was observed between summer DTR and annual NEE in DBF ecosystems (r=−0.33, p<0.05; Figure 4A), while the corresponding correlation in ENF ecosystems was significant and weakly positive (r=0.15, p<0.05; Figure 5A). A partial correlation analysis using the site-level data indicates that the differing response of NEE to summer DTR in the two forest ecosystem types can be attributed to a significant negative (positive) correlation between NEE and T_{max} (T_{min}) in DBF (Figure 4B), while in ENF, the signs of the correlations are reversed (Figure 5B). We further employed a covariance-based structural equation model (CB-SEM) to examine the relationships among summer environmental variables and annual NEE in DBF and ENF ecosystems (Figures 4C & 5C). CB-SEM is advantageous for testing complex theoretical models as it allows for simultaneous estimation of multiple relationships. In DBF, the increases in DTR have had a dual negative impact on NEE, suggesting an enhancement of plant daytime photosynthesis driven by higher daytime temperatures, while the more gradual rises in T_{min} have likely resulted in a comparatively slower increase in nighttime respiration. In ENF ecosystems, the faster increase in T_{max} relative to T_{min} has generally resulted in increased NEE (Figures 5B-C), resulting in a weak positive correlation between DTR and NEE (Figure 5A).

The negative impact of DTR on NEE in DBF can likely be explained by the positive influence of rising daytime temperatures on gross primary production, while the more gradual increase in T_{min} may have resulted in a relatively smaller increase in nighttime respiration. In contrast, daily growth in conifers was more closely linked to daily minimum rather than maximum temperatures, consistent with previous findings.[51-54] A previous study suggests that the cell doubling time of conifers remains relatively stable from 10 to 25°C, but increases exponentially from 50 hours to almost 150 hours as temperatures drop from 10 to 5°C, approaching infinity at 1−2°C.[39] Unlike cell formation, photosynthesis continues at low temperatures, with high assimilation rates maintained even below 5°C.[55-57] This suggests that conifers do not typically depend on higher T_{max} to sustain photosynthesis. In fact, under extreme heat or drought, high T_{max}-induced VPD can increase the water stress on conifers[51] and suppress photosynthesis. This explains the mixed effects of T_{min} (negative) and T_{max} (positive) on NEE in ENF ecosystems. Nevertheless, the positive impact of DTR on NEE in ENF ecosystems remains relatively weak. Thus, despite the positive correlation between DTR and NEE in ENF ecosystems, the overall impact of DTR on NEE (NPP) in the humid zones of the extratropical NH is negative (positive), aligning with the positive effects of DTR on NPP in DBF ecosystems.

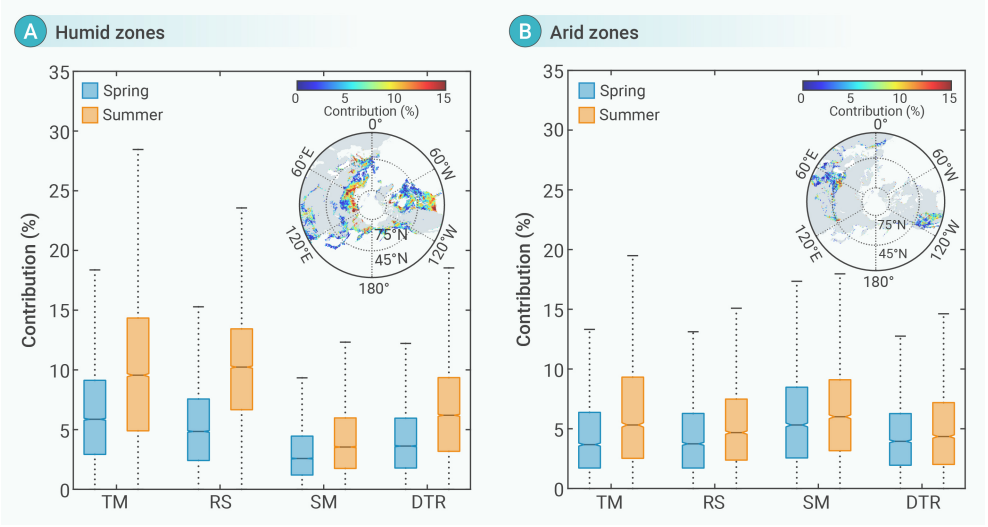

Figure 3. Assessment of the contributions of mean air temperature (TM), solar radiation (RS), soil moisture (SM), and diurnal temperature range (DTR) variations during spring and summer to the variations in annual NPP in humid (A) and arid (B) zones The height of each box represents the interquartile range of contributions for all grid points, with the darker-colored line indicating the median, and the edges denoting the first and third quartiles. Whiskers depict the minimum and maximum contribution values, excluding outliers exceeding 1.5 times the interquartile range. The insets display the spatial distribution of the contribution of summer DTR to annual NPP.

Observations from flux tower sites in grassland and cropland ecosystems within the humid zones indicate no significant linear relationship between DTR and NEE in these ecosystems (Figure S4). One contributing factor is the stronger soil respiration relative to plant respiration in these two ecosystems, leading to high uncertainty in detecting the response of vegetation productivity to changes in DTR. Additionally, intense human activities may interfere with natural factors influencing cropland.[58] In arid zones, the assessment of the impact of summer DTR on annual NEE is hindered by the limited availability of flux tower sites. Focusing on the entire arid and semi-arid zones, we found a significant positive linear relationship between summer DTR and annual NEE within grassland ecosystems (Figure S5). Additionally, after accounting for the influence of summer mean T_{min}, we detected a significant negative partial correlation in grassland ecosystems between summer mean T_{max} and annual gross primary production (r_p=−0.22, p<0.1), and a positive partial correlation with NEE (r_p=0.22, p<0.1). These results imply that daytime warming may constrain productivity and carbon sequestration in local grasslands, possibly due to more water-limited conditions associated with increased VPD and evapotranspiration.

DISCUSSION

Robustness of results

The impact of average temperature increase on vegetation productivity appears to be diminishing in the backdrop of global warming.[44,59,60] Our research, however, illuminates another facet of temperature dynamics over the past two decades—namely, expanding DTR—which is playing a major role in shaping the carbon sequestration capacity of vegetation in the extratropical NH. We conducted a further investigation into the potential responses of vegetation productivity to changes in DTR based on flux tower observations in forested areas. Vegetation productivity is closely linked to NEE, particularly within forest ecosystems.[61-63] We found that in regions where the annual NPP responded positively to summer DTR changes, flux observations indicate a corresponding negative response in annual NEE to summer DTR (Figure S6). Conversely, in areas where the annual NPP exhibited a negative response to summer DTR, NEE similarly displayed a positive response. Utilizing NEE data upscaled using machine learning methods,[20] we found that NEE and NPP show similar responses (with opposite signs) to summer DTR, with a spatial correlation coefficient of r=−0.45 (Figure S7A). This finding supports the contrasting vegetation productivity responses in arid and humid zones, as an increase in NPP typically strengthens the ecosystem's carbon sink capacity, reflected as a decline in NEE.

Similar contrasting responses were detected when using solar-induced fluorescence (SIF)[18] or the kernel normalized difference vegetation index (kNDVI)[19] as indicators of vegetation productivity. The spatial correlation with the NPP responses was r=0.71 for SIF (Figure S8A) and r=0.66 for kNDVI (Figure S8D). To ensure the robustness of our analysis, we also applied principal component regression (PCR)[30] as an additional statistical method. PCR generates principal components that are orthogonal (i.e., uncorrelated) to each other, allowing for optimal performance when dealing with highly correlated predictor variables.[31,32] This method confirmed a consistent pattern in the response of NPP to DTR, showing a high spatial correlation (r=0.84) with the NPP responses identified through ridge regression (Figure S8G). These findings are consistent with previous research indicating that T_{max} and vegetation indices are positively correlated in most wet ecosystems across boreal regions, but negatively correlated in dry temperate regions.[10] Additionally, we found that asymmetric warming between day and night has been most pronounced during the summer season in the extratropical NH. The contributions of summer DTR changes in both humid and arid zones to the annual NPP variation is comparable to the effect of spring temperature variations. Similar contribution magnitudes of DTR to vegetation productivity were obtained through the quantification of predictor importance from both PCR (Figures S8H–I) and random forest analyses (Figures S8J–K), and when using SIF (Figures S8B–C), kNDVI (Figures S8E–F), or NEE (Figures S8B–C) as the indicator of vegetation productivity instead of NPP.

Here, we chose annual vegetation productivity as the response variable instead of monthly or seasonal values due to the substantial uncertainties associated with estimating NPP at shorter time scales. The NPP product from MODIS is derived from gross primary production by subtracting autotrophic respiration, which includes the growth and maintenance respiration of leaves, stems, and roots—processes that are inherently complex[64,65] and vary significantly across seasons and longer timescales.[66]These factors make accurately scaling and modeling autotrophic respiration at shorter intervals highly challenging.[67] Moreover, using annual NPP allows for the capture of carryover effects of environmental variables.[13,14] To further account for the possibility of carryover effects, we performed additional analyses that incorporated environmental variables from both the current year and previous year's seasons as predictors. These analyses produced consistent spatial patterns of the annual NPP response to summer DTR (Figure S9A) and similar magnitudes of DTR contributions to vegetation productivity (Figures S9B–C), reinforcing the robustness of our conclusions. However, it is important to note that using seasonal variables as independent variables and annual variables as the dependent variable may introduce some uncertainty due to the high correlation among independent variables. To further enhance the reliability of our findings, we conducted additional analyses using environmental variables from the growing season (May–October) as independent variables and growing season NEE as the dependent variable. The results further confirm the contrasting responses of vegetation productivity to DTR changes in arid and humid zones (Figure S10) and reveal distinct responses of NEE to DTR in deciduous broadleaf forests and evergreen needleleaf forests (Figure S11).

Mechanisms underlying divergent NPP responses to DTR changes in arid and humid zones

The contrasting effects of increased DTR on vegetation productivity between arid and humid zones suggest that daytime warming limits productivity and carbon sequestration in water-limited environments, where elevated T_{max} drive higher VPD and evapotranspiration, intensifying moisture stress. To reveal the potential effects of DTR changes on VPD, we analyzed half-hourly

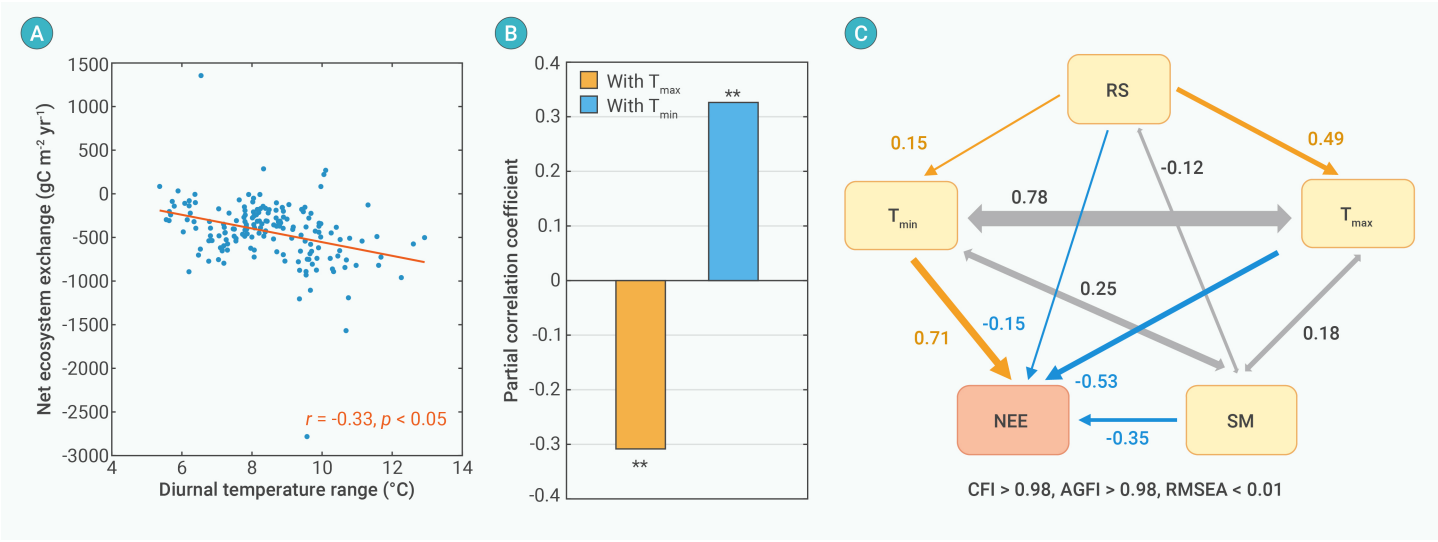

Figure 4. Impact of summer diurnal temperature range (DTR) on annual net ecosystem exchange (NEE) in deciduous broadleaf forest (DBF) ecosystems in humid zones during 2002–2021 (A) Relationship between summer DTR and annual NEE. Each dot represents the annual NEE (y-axis) corresponding to the summer mean DTR (x-axis) across all sites and years within the ecosystem type. The Pearson correlation coefficient (*r*) is shown in the lower part of the figure. (B) Partial correlation coefficient of annual NEE with summer mean daily maximum temperature (T_{max}) or daily minimum temperature (T_{min}), while controlling for the other temperature. The asterisk indicates the significance level (*: p<0.05, **: p<0.01). (C) The hypothesized effects of summer solar radiation (RS), soil moisture (SM), T_{max} and T_{min} on annual NEE, based on structural equation modeling. Double-headed gray arrows denote covariance between variables, while single-headed arrows indicate one-way causation, with positive and negative relationships in yellow and blue, respectively. Arrow thicknesses correspond to the strength of the relationships, with numbers next to the arrows representing the magnitude of the direct coefficients. The numbers below the graphs show the comparative fit index (CFI), adjusted goodness of fit index (AGFI) and root mean square error of approximation (RMSEA) of the structural equation models.

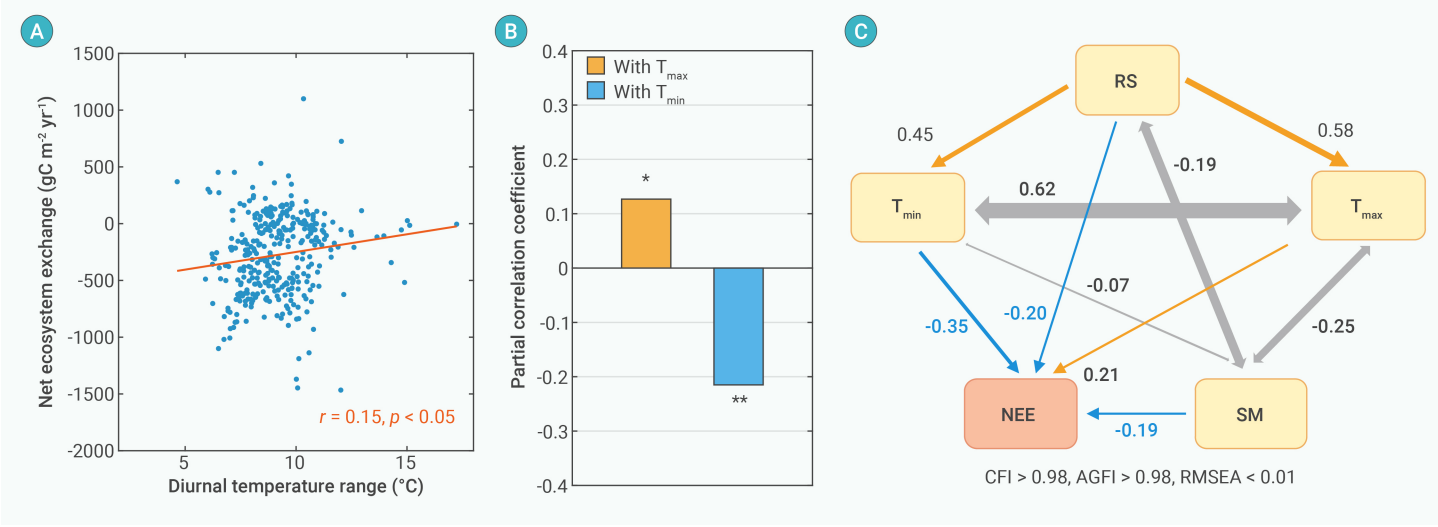

Figure 5. Impact of summer diurnal temperature range (DTR) on annual net ecosystem exchange (NEE) in evergreen needleleaf forest (ENF) ecosystems in humid zones during 2002–2021 (A) Relationship between summer DTR and annual NEE. Each dot represents the annual NEE (y-axis) corresponding to the summer mean DTR (x-axis) across all sites and years within the ecosystem type. The Pearson correlation coefficient (*r*) is shown in the lower part of the figure. (B) Partial correlation coefficient of annual NEE with summer mean daily maximum temperature (T_{max}) or daily minimum temperature (T_{min}), while controlling for the other temperature. The asterisk indicates the significance level (*: p<0.05, **: p<0.01). (C) The hypothesized effects of summer solar radiation (RS), soil moisture (SM), T_{max} and T_{min} on annual NEE, based on structural equation modeling. Double-headed gray arrows denote covariance between variables, while single-headed arrows indicate one-way causation, with positive and negative relationships in yellow and blue, respectively. Arrow thicknesses correspond to the strength of the relationships, with numbers next to the arrows representing the magnitude of the direct coefficients. The numbers below the graphs show the comparative fit index (CFI), adjusted goodness of fit index (AGFI) and root mean square error of approximation (RMSEA) of the structural equation models.

observations of air temperature and VPD from flux tower sites during the summer season (Figure 6A). VPD shows substantial diurnal variations, typically reaching minimum values between 0500 and 0600 local solar time (LST) and peaking between 1400 and 1500 LST in both arid/semi-arid and semi-humid/humid zones (Figures 6B–C). This diurnal cycle in VPD primarily arises from diurnal temperature changes, as indicated by the median R^2 of linear regressions between mean diurnal variations in temperature and VPD, which reaches 98% in both arid/semi-arid and semi-humid/humid zones (Figures 6B–C). The presence of this diurnal cycle suggests that changes in VPD during daytime ($VPD_{daytime}$) and nighttime ($VPD_{nighttime}$) may have different effects on the daily average VPD. Ridge regression and random forest regression analyses based on daily observations reveal that both the ridge regression coefficients of $VPD_{daytime}$ on daily average VPD, and the out-of-bag prediction error estimation of the random forest model, are significantly higher than those of $VPD_{nighttime}$ on daily average VPD (p<0.001, Student's *t*-test; Figure S12). This suggests that $VPD_{daytime}$ exerts a greater influence on daily average VPD changes than $VPD_{nighttime}$. Therefore, DTR increases driven by accelerated daytime temperatures or T_{max} tend to result in elevated daily average VPD.

The above analysis elucidates a potential mechanism by which DTR changes impact VPD. Moreover, the larger diurnal cycle of VPD in arid zones compared to humid zones (Figures 6B–C) indicates that there may be differences in the extent to which DTR changes have affected VPD between these two zones. To quantify the potential impact of DTR changes on VPD, we used

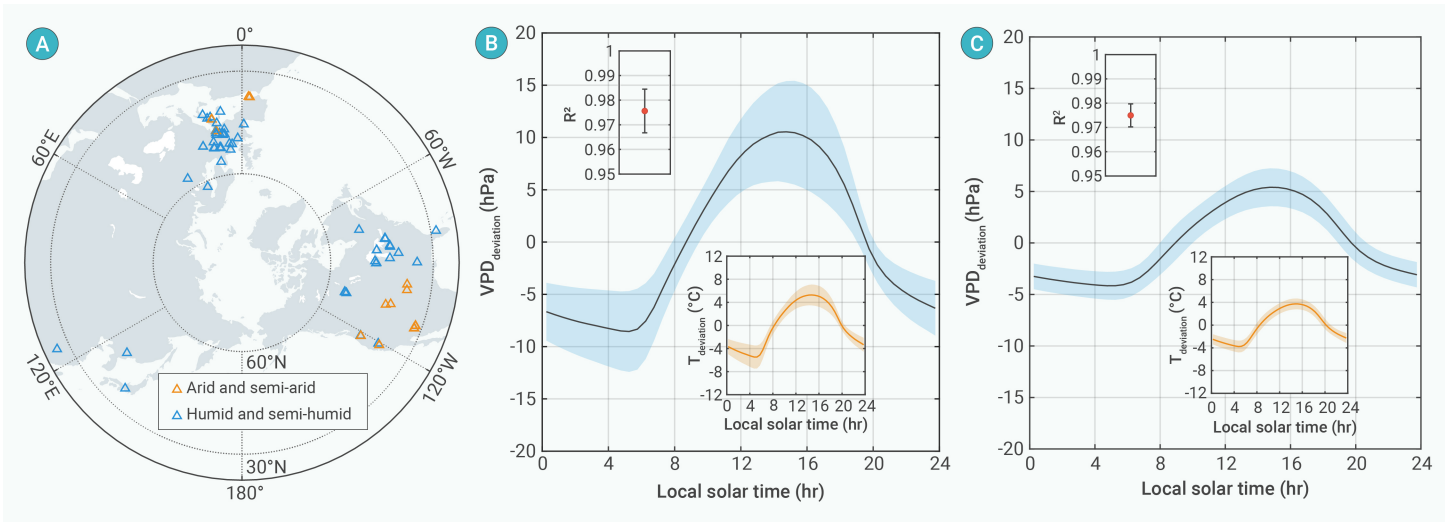

Figure 6. Averaged summer diurnal variations in vapor pressure deficit (VPD) and temperature during 2002–2021 (A) Locations of flux tower sites in arid/semi-arid and semi-humid/humid zones. (B) and (C) Averaged summer diurnal variations in VPD in arid/semi-arid zones (B) and semi-humid/humid zones (C). The y-axis represents the summer-average half-hourly VPD deviations ($VPD_{deviation}$) from the daily mean. The thick lines represent the mean value and the shading the standard deviation around the mean for different sites within each zone. The insets display the summer-average half-hourly temperature deviations ($T_{deviation}$) from the daily mean. The R-squared value (R^2) for the regression of average diurnal variations in temperature on average diurnal variations in VPD is depicted in the upper left, with the mean value and 95% confidence interval displayed by red dots and error bars, respectively.

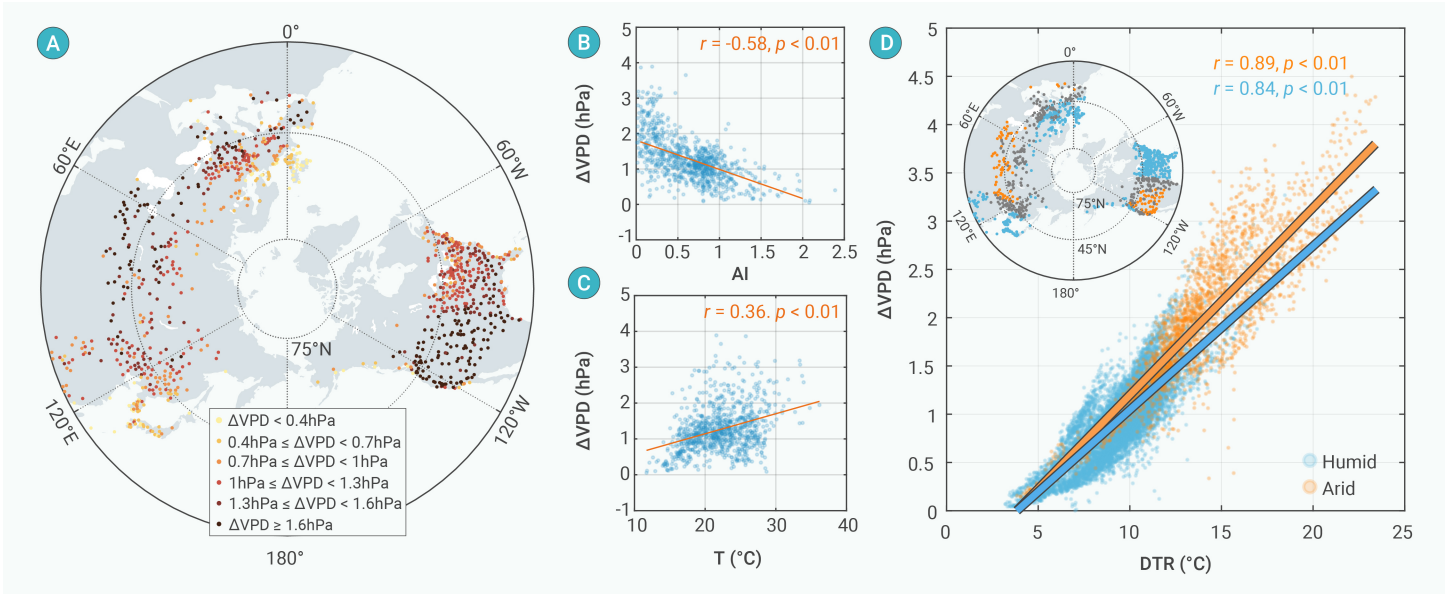

Figure 7. Vapor pressure deficit (VPD) variation and its relationship with changes in diurnal temperature range (DTR) during 2002–2021 (A) Spatial distribution of multi-year (2002–2021) summer average ΔVPD, defined as the difference between daily average VPD calculated using sub-daily temperature and relative humidity, and daily VPD calculated using daily average temperature (T) and relative humidity. The variable ΔVPD is an indicator of the asymmetric effect of sub-diurnal temperature variations on daily average VPD. Observations of temperature and relative humidity were taken from the HadISD dataset. (B) and (C) The relationship between the multi-year summer average ΔVPD and aridity index (AI, B) or multi-year summer average T (C), with the Pearson correlation coefficient (*r*) displayed. (D) Relationship between summer DTR and ΔVPD in arid and humid zones. Each dot represents the summer average ΔVPD (y-axis) corresponding to the summer average DTR (x-axis) across all sites and years (2002–2021) within the arid and humid zones. The inset displays the locations of the observations in arid (yellow point), humid (blue point), and semi-arid/semi-humid (gray point) zones.

two methods to calculate daily VPD based on sub-daily (3-hourly or hourly)[8] temperature and relative humidity data from the in-situ HadISD dataset.[27] In the first method, we calculated VPD at sub-daily intervals and averaged these values to obtain the daily mean VPD ($VPD_{subdaily\rightarrow daily}$). In the second method, we calculated VPD_{daily} directly using daily mean temperature and relative humidity values. The difference between $VPD_{subdaily\rightarrow daily}$ and VPD_{daily}, referred to as ΔVPD, represents the effect of sub-diurnal temperature variations on the daily average VPD. This difference primarily arises from the nonlinear relationship between VPD and temperature.

We found that ΔVPD was generally positive (Figure 7A), revealing a systematic underestimation of VPD when using daily average temperature and relative humidity for its calculation. As expected, there is a strong positive correlation between DTR and ΔVPD(r=0.92, p<0.01, Figure S13A). Spatially, ΔVPD exhibits higher values in arid zones compared to humid zones. Due to the negative correlation between the aridity index (AI) and DTR (Figure S13B) and the positive correlation between DTR and ΔVPD, ΔVPD significantly decreases with increasing AI (r=−0.58, p<0.01, Figure 7B). Beyond its negative relationship with AI, ΔVPD also exhibits a positive correlation with mean temperature (r=0.36, p<0.01, Figure 7C). Based on the Clausius–Clapeyron relation, higher baseline temperatures in arid zones can amplify increases in saturation vapor pressure, resulting in larger increases in VPD. In arid zones, the linear increase in ΔVPD per unit DTR increase (0.15 hPa °C^{-1}) is about 25% higher than in humid zones (0.12 hPa °C^{-1}; Figure 7D). Consequently, $VPD_{subdaily\rightarrow daily}$ in arid zones can increase more rapidly with rising DTR (0.66 hPa °C^{-1}) compared to humid zones (0.56 hPa °C^{-1}, p<0.01; Figure S14). These findings suggest that compared to humid zones, DTR increases in arid zones lead to greater increases in VPD. Combined with recent findings that increased VPD negatively impacts vegetation productiv-

ity in arid zones while it may have neutral effects in humid zones,[31,68] the inhibition of vegetation productivity due to broadening DTR is stronger in the arid zone than the humid zone due to asymmetric effects on VPD.

The above findings shed light on an unresolved question: why increasing T_{min}, which correlates with decreasing DTR, has positively impacted productivity in primarily arid zones.[10,11] Previous research has shown that in humid regions, the negative effect of rising air temperature on SIF—primarily through increased VPD, which inhibits vegetation productivity—has reached nearly 40% of the positive effect of air temperature on SIF. In contrast, in arid zones, the negative effect of rising air temperature through increased VPD was almost 125% of the direct positive effect of rising air temperature on SIF.[31] These findings suggest that in most cases, temperature increases in humid zones tend to enhance vegetation productivity, whereas in arid zones, the negative impact of VPD increase, driven by rising temperatures, outweighs the positive effect of temperature on vegetation productivity. Here we found that an increase in DTR leads to a rise in VPD in both arid and humid zones. In humid zones, the negative effect of VPD increase on vegetation productivity is relatively small and is likely far outweighed by the positive effect of daytime temperature increases on photosynthesis. However, in arid zones, the nonlinear response of VPD to temperature increases means that a unit increase in DTR results in a greater rise in VPD compared to humid zones. Additionally, since the negative impact of rising VPD on vegetation productivity outweighs the positive effects caused by rising temperature in arid zones, increasing daytime temperature and DTR have had an overall negative influence on vegetation productivity in these areas.

Limitations and implications

Changes in DTR resulting from asymmetric warming between day and night may affect vegetation productivity not only by directly influencing photosynthesis and respiration, but also indirectly by impacting events that suppress vegetation productivity, such as fires[69,70] and droughts.[71,72] Furthermore, while the overall increase in summer DTR is most notable, there are also significant trends of increased DTR in spring or autumn in specific locations, potentially impacting local vegetation phenology,[58,73,74] and consequently, vegetation productivity. In-depth investigation aimed at comprehensively assessing and understanding the effects of recent non-uniform climate warming on terrestrial ecosystems from various perspectives is still pending. Considering the substantial impact of northern boreal and temperate forests on the global carbon sink,[63,75] particular attention should be directed towards understanding the response of northern ecosystems to recent asymmetric warming dynamics. Notably, our findings suggest that VPD calculated using daily mean temperature and relative humidity tends to underestimate the true daily mean VPD across most land regions. Given the influence of diurnal temperature variation on VPD, future studies should incorporate both T_{max} and T_{min} in VPD calculations to achieve more accurate assessments.

Due to the current limitations of Earth system models in accurately simulating trends in DTR,[8] a skillful prediction of future DTR variation and its influence on the spatial distribution patterns of vegetation productivity presents a substantial challenge that lies ahead. Here, we have reported opposing collective influences of DTR, air temperature, and solar radiation variations on NPP in humid and arid zones in the extratropical NH over the recent two decades. If these relationships persist, future increases in DTR—possibly in conjunction with global warming and brightening—[76,77] could further widen the vegetation productivity gap between extratropical NH humid and arid zones, highlighting the need for careful consideration and attention.

REFERENCES

1. Tokarska K. B., Stolpe M. B., Sippel S., et al. (2020). Past warming trend constrains future warming in CMIP6 models. *Sci. Adv.* **6**:eaaz9549. DOI:10.1126/sciadv.aaz9549
2. Samset B. H., Zhou C., Fuglestvedt J. S., et al. (2022). Earlier emergence of a temperature response to mitigation by filtering annual variability. *Nat. Commun.* **13**:1578. DOI:10.1038/s41467-022-29247-y
3. Xu L., Myneni R. B., Chapin Iii F. S., et al. (2013). Temperature and vegetation seasonality diminishment over northern lands. *Nat. Clim. Change* **3**:581–586. DOI:10.1038/nclimate1836
4. Mann M. E. and Park J. (1996). Greenhouse warming and changes in the seasonal cycle of temperature: Model versus observations. *Geophys. Res. Lett.* **23**:1111-1114. DOI:10.1029/96GL01066
5. Easterling D. R., Horton B., Jones P. D., et al. (1997). Maximum and Minimum Temperature Trends for the Globe. *Science* **277**:364–367. DOI:10.1126/science.277.5324.364
6. Braganza K., Karoly D. J. and Arblaster J. M. (2004). Diurnal temperature range as an index of global climate change during the twentieth century. *Geophys. Res. Lett.* **31**. DOI:10.1029/2004GL019998
7. Zhong Z., He B., Chen H. W., et al. (2023). Reversed asymmetric warming of subdiurnal temperature over land during recent decades. *Nat. Commun.* **14**:7189. DOI:10.1038/s41467-023-43007-6
8. Huang X., Dunn R. J. H., Li L. Z. X., et al. (2023). Increasing Global Terrestrial Diurnal Temperature Range for 1980–2021. *Geophys. Res. Lett.* **50**:e2023GL103503. DOI:10.1029/2023GL103503
9. Dai A., Genio A. D. D. and Fung I. Y. (1997). Clouds, precipitation and temperature range. *Nature* **386**:665–666. DOI:10.1038/386665b0
10. Peng S., Piao S., Ciais P., et al. (2013). Asymmetric effects of daytime and night-time warming on Northern Hemisphere vegetation. *Nature* **501**:88–92. DOI:10.1038/nature12434
11. Xia J., Chen J., Piao S., et al. (2014). Terrestrial carbon cycle affected by non-uniform climate warming. *Nat. Geosci.* **7**:173–180. DOI:10.1038/ngeo2093
12. Alward R. D., Detling J. K. and Milchunas D. G. (1999). Grassland Vegetation Changes and Nocturnal Global Warming. *Science* **283**:229–231. DOI:10.1126/science.283.5399.229
13. Lian X., Piao S., Chen A., et al. (2021). Seasonal biological carryover dominates northern vegetation growth. *Nat. Commun.* **12**:983. DOI:10.1038/s41467-021-21223-2
14. Lian X., Peñuelas J., Ryu Y., et al. (2024). Diminishing carryover benefits of earlier spring vegetation growth. *Nat. Ecol. Evol.* **8**:218–228. DOI:10.1038/s41559-023-02272-w
15. Zhu G., Wang X., Xiao J., et al. (2022). Daytime and nighttime warming has no opposite effects on vegetation phenology and productivity in the northern hemisphere. *Sci. Total Environ.* **822**:153386. DOI:10.1016/j.scitotenv.2022.153386
16. Zhang X., Rademacher T., Liu H., et al. (2023). Fading regulation of diurnal temperature ranges on drought-induced growth loss for drought-tolerant tree species. *Nat. Commun.* **14**:6916. DOI:10.1038/s41467-023-42654-z
17. Running S. W. and Zhao M. (2019). User's guide daily GPP and annual NPP (MOD17A2H/A3H) and year-end gap-filled (MOD17A2HGF/A3HGF) products NASA earth observing system MODIS land algorithm (for collection 6). *Process. DAAC* **490**:1–37.https://lpdaac.usgs.gov/documents/972/MOD17_User_Guide_V61.pdf
18. Li X. and Xiao J. (2019). A Global, 0.05-Degree Product of Solar-Induced Chlorophyll Fluorescence Derived from OCO-2, MODIS, and Reanalysis Data. *Remote Sens.* **11**:517. DOI:10.3390/rs11050517.
19. Camps-Valls G., Campos-Taberner M., Moreno-Martínez Á., et al. (2021). A unified vegetation index for quantifying the terrestrial biosphere. *Sci. Adv.* **7**:eabc7447. DOI:10.1126/sciadv.abc7447
20. Jung M., Koirala S., Weber U., et al. (2019). The FLUXCOM ensemble of global land-atmosphere energy fluxes. *Sci. Data* **6**:74. DOI:10.1038/s41597-019-0076-8
21. Rohde R. A. and Hausfather Z. (2020). The Berkeley Earth Land/Ocean Temperature Record. *Earth Syst. Sci. Data* **12**:3469–3479. DOI:10.5194/essd-12-3469-2020
22. Gelaro R., McCarty W., Suárez M. J., et al. (2017). The Modern-Era Retrospective Analysis for Research and Applications, Version 2 (MERRA-2). *J. Clim.* **30**:5419-5454. DOI:10.1175/JCLI-D-16-0758.1
23. Martens B., Miralles D. G., Lievens H., et al. (2017). GLEAM v3: satellite-based land evaporation and root-zone soil moisture. *Geosci. Model Dev.* **10**:1903–1925. DOI:10.5194/gmd-10-1903-2017
24. Zomer R. J., Xu J. and Trabucco A. (2022). Version 3 of the Global Aridity Index and Potential Evapotranspiration Database. *Sci. Data* **9**:409. DOI:10.1038/s41597-022-01493-1
25. Pastorello G., Trotta C., Canfora E., et al. (2020). The FLUXNET2015 dataset and the ONEFlux processing pipeline for eddy covariance data. *Sci. Data* **7**. 225. DOI:10.1038/s41597-020-0534-3
26. ICOS (2023). Ecosystem final quality (L2) product in ETC-Archive format - release 2023-1 (Version 1.0). DOI:10.18160/YDH2-VFYE
27. Dunn R. J. H., Willett K. M., Parker D. E., et al. (2016). Expanding HadISD: quality-controlled, sub-daily station data from 1931. *Geosci. Instrum. Method. Data Syst.* **5**:473–491. DOI:10.5194/gi-5-473-2016
28. Smith A., Lott N. and Vose R. (2011). The Integrated Surface Database: Recent Developments and Partnerships. *Bull. Am. Meteorol. Soc.* **92**:704-708. DOI:10.1175/2011BAMS3015.1
29. Dunn R. J. H., Willett K. M., Thorne P. W., et al. (2012). HadISD: a quality-controlled global synoptic report database for selected variables at long-term stations from 1973–2011. *Clim. Past* **8**:1649–1679. DOI:10.5194/cp-8-1649-2012
30. Park S. H. (1981). Collinearity and Optimal Restrictions on Regression Parameters for Estimating Responses. *Technometrics* **23**:289–295. DOI:10.1080/00401706.1981.10487652
31. Zhong Z., He B., Wang Y. P., et al. (2023). Disentangling the effects of vapor pressure deficit on northern terrestrial vegetation productivity. *Sci. Adv.* **9**:eadf3166. DOI:10.1126/sciadv.adf3166
32. Wang X., Ciais P., Wang Y., et al. (2018). Divergent response of seasonally dry tropical

vegetation to climatic variations in dry and wet seasons. *Global Change Biol.* **24**:4709-4717. DOI:10.1111/gcb.14335
33. Makowski K., Jaeger E. B., Chiacchio M., et al. (2009). On the relationship between diurnal temperature range and surface solar radiation in Europe. *J. Geophys. Res.:Atmos.* **114**. DOI:10.1029/2008JD011104
34. Liu B., Xu M., Henderson M., et al. (2004). Taking China's Temperature: Daily Range, Warming Trends, and Regional Variations, 1955–2000. *J. Clim.* **17**:4453-4462. DOI:10.1175/3230.1
35. Liu L., Gudmundsson L., Hauser M., et al. (2020). Soil moisture dominates dryness stress on ecosystem production globally. *Nat. Commun.* **11**:4892. DOI:10.1038/s41467-020-18631-1
36. Stocker B. D., Zscheischler J., Keenan T. F., et al. (2018). Quantifying soil moisture impacts on light use efficiency across biomes. *New Phytol.* **218**:1430-1449. DOI:10.1111/nph.15123
37. Huang M., Piao S., Ciais P., et al. (2019). Air temperature optima of vegetation productivity across global biomes. *Nat. Ecol. Evol.* **3**:772–779. DOI:10.1038/s41559-019-0838-x
38. Chen W., Wang S., Wang J., et al. (2023). Evidence for widespread thermal optimality of ecosystem respiration. *Nat. Ecol. Evol.* **7**:1379–1387. DOI:10.1038/s41559-023-02121-w
39. Körner C. (2003). Carbon limitation in trees. *J. Ecol.* **91**:4-17. DOI:10.1046/j.1365-2745.2003.00742.x
40. Donohue R. J., McVicar T. R. and Roderick M. L. (2010). Assessing the ability of potential evaporation formulations to capture the dynamics in evaporative demand within a changing climate. *J. Hydrol.* **386**:186-197. DOI:10.1016/j.jhydrol.2010.03.020
41. Ek M. B. and Holtslag A. A. M. (2004). Influence of Soil Moisture on Boundary Layer Cloud Development. *J. Hydrometeorol.* **5**:86-99. DOI:10.1175/1525-7541(2004)005<0086:IOSMOB>2.0.CO;2
42. Dai A., Trenberth K. E. and Karl T. R. (1999). Effects of Clouds, Soil Moisture, Precipitation, and Water Vapor on Diurnal Temperature Range. *J. Clim.* **12**:2451-2473. DOI:10.1175/1520-0442(1999)012<2451:EOCSMP>2.0.CO;2
43. Yuan W., Zheng Y., Piao S., et al. (2019). Increased atmospheric vapor pressure deficit reduces global vegetation growth. *Sci. Adv.* **5**:eaax1396. DOI:10.1126/sciadv.aax1396
44. Zhang Y., Piao S., Sun Y., et al. (2022). Future reversal of warming-enhanced vegetation productivity in the Northern Hemisphere. *Nat. Clim. Change* **12**:581–586. DOI:10.1038/s41558-022-01374-w
45. Running S. W., Nemani R. R., Heinsch F. A., et al. (2004). A Continuous Satellite-Derived Measure of Global Terrestrial Primary Production. *BioScience* **54**:547–560. DOI:10.1641/0006-3568(2004)054[0547:Acsmog]2.0.Co;2
46. Barnes M. L., Zhang Q., Robeson S. M., et al. (2024). A Century of Reforestation Reduced Anthropogenic Warming in the Eastern United States. *Earth's Future* **12**:e2023EF003663. DOI:10.1029/2023EF003663
47. Roby M. C., Scott R. L. and Moore D. J. P. (2020). High Vapor Pressure Deficit Decreases the Productivity and Water Use Efficiency of Rain-Induced Pulses in Semiarid Ecosystems. *J. Geophys. Res.:Biogeosci.* **125**:e2020JG005665. DOI:10.1029/2020JG005665
48. Li F., Xiao J., Chen J., et al. (2023). Global water use efficiency saturation due to increased vapor pressure deficit. *Science* **381**:672–677. DOI:10.1126/science.adf5041
49. He B., Chen C., Lin S., et al. (2021). Worldwide impacts of atmospheric vapor pressure deficit on the interannual variability of terrestrial carbon sinks. *Natl. Sci. Rev.* **9**. DOI:10.1093/nsr/nwab150
50. Ma H., Crowther T. W., Mo L., et al. (2023). The global biogeography of tree leaf form and habit. *Nat. Plants* **9**:1795–1809. DOI:10.1038/s41477-023-01543-5
51. Deslauriers A., Morin H., Urbinati C., et al. (2003). Daily weather response of balsam fir (Abies balsamea (L. *) Mill.) stem radius increment from dendrometer analysis in the boreal forests of Québec (Canada). Trees* **17**:477–484. DOI:10.1007/s00468-003-0260-4
52. Xiong W., Wang Y., Yu P., et al. (2007). Growth in stem diameter of Larix principis-rupprechtii and its response to meteorological factors in the south of Liupan Mountain, China. *Acta Ecol. Sin.* **27**:432-440. DOI:10.1016/S1872-2032(07)60015-8
53. Rossi S., Deslauriers A., Griçar J., et al. (2008). Critical temperatures for xylogenesis in conifers of cold climates. *Global Ecol. Biogeogr.* **17**:696-707. DOI:10.1111/j.1466-8238.2008.00417.x
54. Xiao X., Hollinger D., Aber J., et al. (2004). Satellite-based modeling of gross primary production in an evergreen needleleaf forest. *Remote Sens. Environ.* **89**:519-534. DOI:10.1016/j.rse.2003.11.008
55. Tranquillini W. (1979). Physiological ecology of the alpine timberline: tree existence at high altitudes with special reference to the European Alps (Springer Berlin, Heidelberg). 10.1007/978-3-642-67107-4
56. Pisek A. and Winkler E. (1958). Assimilationsvermögen und Respiration der Fichte (Picea excelsa Link) in verschiedener Höhenlage und der Zirbe (Pinus cembra L.) an der alpinen Waldgrenze. *Planta* **51**:518–543. https://www.jstor.org/stable/23363415
57. Körner C. (1998). A re-assessment of high elevation treeline positions and their explanation. *Oecologia* **115**:445-459. DOI:10.1007/s004420050540
58. Liu Y., Wu C., Wang X., et al. (2023). Contrasting responses of peak vegetation growth to asymmetric warming: Evidences from FLUXNET and satellite observations. *Global Change Biol.* **29**:2363-2379. DOI:10.1111/gcb.16592
59. Piao S., Nan H., Huntingford C., et al. (2014). Evidence for a weakening relationship between interannual temperature variability and northern vegetation activity. *Nat. Commun.* **5**:5018. DOI:10.1038/ncomms6018
60. Wang K., Bastos A., Ciais P., et al. (2022). Regional and seasonal partitioning of water and temperature controls on global land carbon uptake variability. *Nat. Commun.* **13**:3469. DOI:10.1038/s41467-022-31175-w
61. Stuart-Haëntjens E. J., Curtis P. S., Fahey R. T., et al. (2015). Net primary production of a temperate deciduous forest exhibits a threshold response to increasing disturbance severity. *Ecology* **96**:2478-2487. DOI:10.1890/14-1810.1
62. Norby R. J., DeLucia E. H., Gielen B., et al. (2005). Forest response to elevated CO_2 is conserved across a broad range of productivity. *Proc. Natl. Acad. Sci.* **102**:18052–18056. DOI:10.1073/pnas.0509478102
63. Pan Y., Birdsey R. A., Fang J., et al. (2011). A Large and Persistent Carbon Sink in the World's Forests. *Science* **333**:988–993. DOI:10.1126/science.1201609
64. Franklin O., Johansson J., Dewar R. C., et al. (2012). Modeling carbon allocation in trees: a search for principles. *Tree Physiol.* **32**:648–666. DOI:10.1093/treephys/tpr138
65. Fatichi S., Pappas C., Zscheischler J., et al. (2019). Modelling carbon sources and sinks in terrestrial vegetation. *New Phytol.* **221**:652-668. DOI:10.1111/nph.15451
66. Grünzweig J. M., Hemming D., Maseyk K., et al. (2009). Water limitation to soil CO2 efflux in a pine forest at the semiarid "timberline". *J. Geophys. Res.:Biogeosci.* **114**. DOI:10.1029/2008JG000874
67. Klein T. and Hoch G. (2015). Tree carbon allocation dynamics determined using a carbon mass balance approach. *New Phytol.* **205**:147-159. DOI:10.1111/nph.12993.
68. Chen N., Zhang Y., Yuan F., et al. (2023). Warming-induced vapor pressure deficit suppression of vegetation growth diminished in northern peatlands. *Nat. Commun.* **14**:7885. DOI:10.1038/s41467-023-42932-w
69. Balch J. K., Abatzoglou J. T., Joseph M. B., et al. (2022). Warming weakens the night-time barrier to global fire. *Nature* **602**:442–448. DOI:10.1038/s41586-021-04325-1
70. Luo K., Wang X., de Jong M., et al. (2024). Drought triggers and sustains overnight fires in North America. *Nature* **627**:321–327. DOI:10.1038/s41586-024-07028-5
71. Wang X. and Wang X. (2024). Hotter drought and trade-off between fast and slow growth strategies as major drivers of tree-ring growth variability of global conifers. *J. Ecol.* **112**. DOI:10.1111/1365-2745.14290
72. Bottero A., Forrester D. I., Cailleret M., et al. (2021). Growth resistance and resilience of mixed silver fir and Norway spruce forests in central Europe: Contrasting responses to mild and severe droughts. *Global Change Biol.* **27**:4403-4419. DOI:10.1111/gcb.15737
73. Piao S., Tan J., Chen A., et al. (2015). Leaf onset in the northern hemisphere triggered by daytime temperature. *Nat. Commun.* **6**:6911. DOI:10.1038/ncomms7911
74. Wu C., Wang X., Wang H., et al. (2018). Contrasting responses of autumn-leaf senescence to daytime and night-time warming. *Nat. Clim. Change* **8**:1092–1096. DOI:10.1038/s41558-018-0346-z
75. Yang H., Ciais P., Frappart F., et al. (2023). Global increase in biomass carbon stock dominated by growth of northern young forests over past decade. *Nat. Geosci.* **16**:886–892. DOI:10.1038/s41561-023-01274-4
76. Wild M., Gilgen H., Roesch A., et al. (2005). From Dimming to Brightening: Decadal Changes in Solar Radiation at Earth's Surface. *Science* **308**:847–850. DOI:10.1126/science.1103215
77. Wild M. (2012). Enlightening Global Dimming and Brightening. *Bull. Am. Meteorol. Soc.* **93**:27-37. DOI:10.1175/BAMS-D-11-00074.1

FUNDING AND ACKNOWLEDGMENTS

The study was supported by internal funding from Chalmers University of Technology. Z.Z. was supported by the VAPOR project (grant number 101154385), funded by the Horizon Europe, MSCA Postdoctoral Fellowships 2023. H.W.C. was supported by the Swedish National Space Agency, grant number 2021-00149. The funders had no role in study design, data collection and analysis, decision to publish, or preparation of the manuscript.

AUTHOR CONTRIBUTIONS

Z.Z. designed the research, performed the analysis and wrote the draft; H.W.C., B.H. and B.S. provided comments to improve the manuscript; H.W.C. supervised the project. All authors contributed to the manuscript and approved the final version.

DECLARATION OF INTERESTS

The authors declare no competing interests.

DATA AND CODE AVAILABILITY

All datasets that support the findings of this study are publicly available. Data are freely accessible from the following sources: the MODIS NPP and NDVI datasets are from https://modis.gsfc.nasa.gov/data/. The GOSIF dataset is from https://globalecology.unh.edu/data/GOSIF.html. The FLUXCOM NEE dataset is from http://fluxcom.org/. The BEST dataset is from https://berkeleyearth.org/data/. The GLEAM soil moisture dataset is from https://www.gleam.eu/#datasets. The aridity index dataset is from https://doi.org/10.6084/m9.figshare.7504448.v5. The FLUXNET2015 dataset is from https://fluxnet.org/

data/fluxnet2015-dataset/. The ICOS dataset is from https://www.icos-cp.eu/data-products. The HadISD dataset is from https://www.metoffice.gov.uk/hadobs/hadisd/. The MERRA-2 downwards shortwave radiation is from https://disc.gsfc.nasa.gov/datasets?project=MERRA-2. Code is available from the corresponding author upon reasonable request.

SUPPLEMENTAL INFORMATION

It can be found online at https://doi.org/10.59717/j.xinn-geo.2025.100163